



ELSEVIER

Available online at www.sciencedirect.com

SCIENCE @ DIRECT®

Global and Planetary Change 45 (2005) 313–332

GLOBAL AND PLANETARY
CHANGE

www.elsevier.com/locate/gloplacha

Primary production of Inner Mongolia, China, between 1982 and 1999 estimated by a satellite data-driven light use efficiency model

Sara Brogaard^{a,*}, Micael Runnström^{a,1}, Jonathan W. Seaquist^{b,2}

^aDepartment of Physical Geography and Ecosystems Analysis, Lund University, Sölvegatan 13, 22362 Lund, Sweden

^bDepartment of Geography and McGill Centre for Global and Climate Change Research, McGill University, 805 Sherbrooke St. West, Montreal, Quebec, Canada H3A 2K6

Received 2 July 2003; accepted 24 September 2004

Abstract

Declining biological production as a part of an ongoing land degradation process is considered a severe environmental problem in the dry northern and northwestern regions of China. The aim of this study is to develop and adapt a satellite data-driven gross primary production model called Lund University light use efficiency model (LULUE) to temperate conditions in order to map gross primary production (GPP) for the Grasslands of Inner Mongolia Autonomous Region (IMAR), China, from 1982 to 1999. The water stress factor included in the original model has been complemented with two temperature stress factors. In addition, algorithms that allocate the proportions of C3/C4 photosynthetic pathways used by plants and that compute temperature-based C3 maximum efficiency values have been incorporated in the model.

The applied light use efficiency (LUE) model is using time series of the Normalized Difference Vegetation Index (NDVI), CLOUDS from AVHRR (CLAVR) from the 8-km resolution NOAA Pathfinder Land Data Set (PAL). Quasi-daily rainfall and monthly minimum and maximum temperatures, together with soil texture information, are used to compute water limitations to plant growth. The model treats bare soil evaporation and actual transpiration separately, a refinement that is more biophysically realistic, and leads to enhanced precision in our water stress term, especially across vegetation gradients.

Based on ground measurements of net primary production (NPP) at one site, the LULUE reproduces the variability of primary production better than CENTURY or NDVI alone. Mean annual GPP between 1982 and 1999 range from about 100 g/m² in desert regions in the west to about 4000 g/m² in the northeast of IMAR, and the coefficient of variation for GPP is highest near the margins of the deserts in the west where rainfall is erratic. Linear trends fitted through the 18-year time series reveal that the western regions have encountered no change, while a large area in the center of the IMAR shows marked increases in GPP. In the northeast, negative trends in GPP are noted and coincide with rainfall trends. Though the

* Corresponding author. Present address: Department of Geography and McGill Centre for Global and Climate Change Research, McGill University, Montreal, 805 Sherbrooke St. W. Montreal, Quebec, Canada H3A 2K6. Tel.: +1 514 3983458; fax: +1 514 3987437.

E-mail addresses: brogaard@geog.mcgill.ca (S. Brogaard), micael.runnstrom@nateko.lu.se (M. Runnström), jonathan.seaquist@staff.mcgill.ca (J.W. Seaquist).

¹ Tel.: +46 46 2227925; fax: +46 46 2228391.

² Tel.: +1 514 3984347; fax: +1 514 3984347.

high inter-annual variability in primary production undermines the identification of significant trends, we could not isolate any general decline in grassland primary production.

© 2004 Elsevier B.V. All rights reserved.

Keywords: Primary production; Grassland; NDVI; Light use efficiency (LUE); Inner Mongolia; China

1. Introduction

1.1. Background

Declining biological production as a part of an ongoing land degradation process is considered a severe environmental problem in the dry northern and northwestern regions of China, including the Inner Mongolia Autonomous Region (IMAR) (State Environmental Protection Administration, 2002). The underlying factors are believed to be increasing livestock numbers, expansion of cultivated land on erosive soils and the gathering of fuel wood and herb digging (Zha and Gao, 1997). The Chinese transition towards market economy following the 1978 economic reforms has led to rising living standards, which, in combination with a continued growing population, is assumed to have increased the pressure on marginal lands (e.g., Longworth and Williamson, 1993; Brown, 1995; Thwaites et al., 1998; Ho, 2000). The Chinese state has in recent years intensified land rehabilitation and afforestation efforts although efforts and progress vary across the region (Nyberg and Rozelle, 1999; Yang and Li, 2000; Brogaard and Zhao, 2002; Runnström, 2003). Following particularly severe sand storms in the winter and spring of 2000 and 2001, the possible impact of a changing vegetation cover has been debated (Feng et al., 2001; Cyranoski, 2003). Furthermore, the quantification of the biological productivity is of interest in evaluating the role of the grasslands of China in the global carbon cycle (Ni, 2002). Accordingly, there is a need to study the vegetative development of the IMAR grasslands.

1.2. Objectives

The overall aim of this work is to gain insight into the natural resource situation in IMAR by using an improved gross primary production (GPP) model named Lund University Light Use Efficiency model

(LULUE). More specifically, this aim has been achieved through the following objectives: (1) to adapt a satellite-driven parametric model, originally developed for Sahelian conditions (Seaquist, 2001; Seaquist et al., 2004), to the central Asian steppe region of IMAR by including additional stress factors and growth efficiency computations; (2) to estimate monthly primary production between the years 1982 and 1999. The applied model uses satellite sensor-acquired reflectance in combination with climate data to generate monthly estimates of GPP. The light use efficiency (LUE) concept is useful as it reduces the complexities of plant growth into a simple, yet robust parametric statement and is therefore potentially more powerful than using the Normalized Difference Vegetation Index (NDVI) alone to track primary production. NDVI has been used in studies over longer time periods as an indicator of relative biomass amount (Tucker et al., 1994; Runnström, 2000; Eklundh and Olsson, 2003). A more biophysical approach, as the LUE model enables an estimation of absolute values of primary production. As this study estimates GPP over a 18-year period, it enables, on a cell-by-cell basis, the calculation of (a) mean GPP values for the Inner Mongolian grasslands, (b) its variability and (c) indication of trends.

1.3. The light use efficiency approach

Remotely sensed data from sensors such as the National Oceanographic and Atmospheric Administration Advanced Very High Radiometric Resolution (NOAA AVHRR) are useful for monitoring biological productivity because the reflectance signal can be converted into biophysically meaningful descriptors of the land surface. The LUE approach (Monteith, 1972, 1977) proposes that biological production is directly proportional to the amount of photosynthetically active radiation absorbed by the vegetation canopy (APAR). APAR itself is the product of incident photosynthetically active radiation (PAR)

between 0.4 and 0.7 μm and the reflectance properties expressed through a vegetation index, i.e., the NDVI (Eq. (1)). ε_p refers to the maximum biological efficiency of PAR conversion to dry matter (g/MJ m^2) and ε is an environmental stress scalar. a and b are regression coefficients for deriving the fraction of plant canopy absorbed photosynthetic radiation (FPAR) through the NDVI. NDVI is based on the ratio between the near infrared (NIR) and the red (RED) reflectance proportions of the electromagnetic spectrum (Eq. (2)):

$$\text{GPP} = \sum_{i=1}^n \varepsilon_p \varepsilon (a * \text{NDVI} + b) * \text{PAR} \quad (1)$$

$$\text{NDVI} = (\text{NIR} - \text{RED}) / (\text{NIR} + \text{RED}) \quad (2)$$

GPP represents the amount of energy converted into dry plant matter (allocated in roots, shoot, leaves seeds, etc.) through photosynthesis. To assess the net primary production (NPP), maintenance and growth respiration should be subtracted from GPP. Sensitivity studies with radiation transfer models indicate that the relationship between NDVI and FPAR remains robust in the presence of pixel heterogeneity, vegetation clumping, and variations in leaf orientation and optical properties (Goward and Hummerich, 1992; Myneni and Williams, 1994).

LUE models driven by remotely sensed data have been widely used to map primary production for the terrestrial biosphere as they reduce the fundamental rules governing the biological production to a limited number of parameters (e.g., Law and Warring, 1994, Ruimy et al., 1994, Paruelo et al., 1997, Rasmussen, 1998, Goetz et al., 1999, Nouvellon et al., 2000, Seaquist, 2001). Early LUE approaches assumed constant ε , but it has later been shown to vary, not only between biomes, but also between species, between plants of a particular species and for a single plant over time. These variations may be attributed to short-term environmental stress (Goetz and Prince, 1999). Under short-term environmental stress (e.g., drought, temperature) a reduction in growth appears through a reduction in the efficiency coefficient. These stress factors may be summarized as a scalar ε , which is multiplied with ε_p , hence reducing GPP from its potential in Eq. (1). In the longer term, the stress factors may result in declining leaf area and

interception of radiation, indicated by a reduction in NDVI. In drylands characterized by a short and intensive rainy season with a high degree of inter-annual variability, the biological production is mainly mediated by the spatial and temporal variations in moisture availability. Therefore, water-stress-induced reduction in ε is the main constraint for maximum biological efficiency in these environments (Yusheng et al., 1991; Xiao et al., 1995).

There are a number of LUE-type models of varying complexity described in the literature, some of which use satellite data as a driver (e.g., Goetz et al., 1999), and others that are general enough to be applied to a number of different biomes including grasslands (e.g., Running and Hunt, 1993). The LULUE is similar to some of these to the extent that it is embedded in a LUE framework. On a more detailed level, our approach is unique because it considers only the water used by plants (actual transpiration) to index water stress. This is particularly important for applications in partially vegetated landscapes where the fate of precipitation is highly controlled by relative amounts of vegetation. Our parameterization of water stress is both pragmatic and biophysically realistic.

The accumulation of CO_2 in the atmosphere, about 9% between 1980 and 2000 (Nemani et al., 2003), is not dealt with specifically in this model. The CO_2 fertilization feedback effect on production is assumed to manifest itself through the NDVI.

2. Materials and methods

2.1. Site description

The IMAR occupies almost 1,200,000 km^2 of China's northern and northeastern regions. The climate is dominated by the monsoon, which is controlled by the Eurasian continental high- and low-pressure cells and experience winters that are dry and cold with strong northwesterly winds regulated by the Siberia–Mongolian high cold atmospheric pressure cell. During the summer months, the circulation is reversed, bringing warm and humid air masses from the Pacific, resulting in high temperatures and limited and varying rainfall. A majority of the IMAR lies in the arid and semi-arid climate zones where annual precipitation ranges from less than 100

mm in the arid west to about 500 mm in the east (Zhu et al., 1986). The dominant land use activity in the dry steppes of the IMAR is animal husbandry, and the total livestock number, registered at the end of June, has increased from about 46 million head to about 71 million between 1980 and 1997 (Statistical yearbook of Inner Mongolia, 1998). In the agro-pastoral transition zone, cultivation is enlarged and intensified through an increased use of fertilizers and pesticides, and irrigation is expanding (Brogaard and Zhao, 2002; Runnström, 2003). The northeastern part of the IMAR is mountainous, producing orographic precipitation and the vegetation is dominated by broad-leaf and needle-leaf forests (Fig. 1).

Grassland resources vary with topography, soil, ground water level, human and animal impact, etc., and range from good vegetation cover of quality grasses consisting of, e.g., *Caragana intermedia* and *Hedysarum scoparium*, to less vegetated areas with *Stipa breviflora*, *Artemisia frigida* and *Caragana* shrubs (Grassland and Grassland Sciences in North-

ern China, 1992). Sparsely vegetated areas consisting of sand dunes form sandy lands (*shamo*) that are often patchy mixtures of dunes and grassland, e.g., the Mu Us, on the Ordos Plateau and the Keerqin steppe (marked in Fig. 1). For these two areas, used as reference sites in this paper, more thorough reports have been presented in Runnström (2000), Brogaard and Zhao (2002) and Runnström (2003). They both represent semi-arid steppe with intensive usage and also have a denser representation of climate stations. One grid cell of 8 km in each of these areas was used for analyses of modeled GPP and controls. The Mu Us is represented by a grid cell (39°05'N, 107°44'E), about 25 km west of the Eutoke climate station, with an annual average precipitation of 273 mm, and the Keerqin steppe (43.00°N, 120.49°E), about 15 km north and 10 km east of Naiman climate station, receiving 398 mm. Moving the grid cell from the exact position of the climate station was done to avoid other land use as urbanized and cultivated areas.

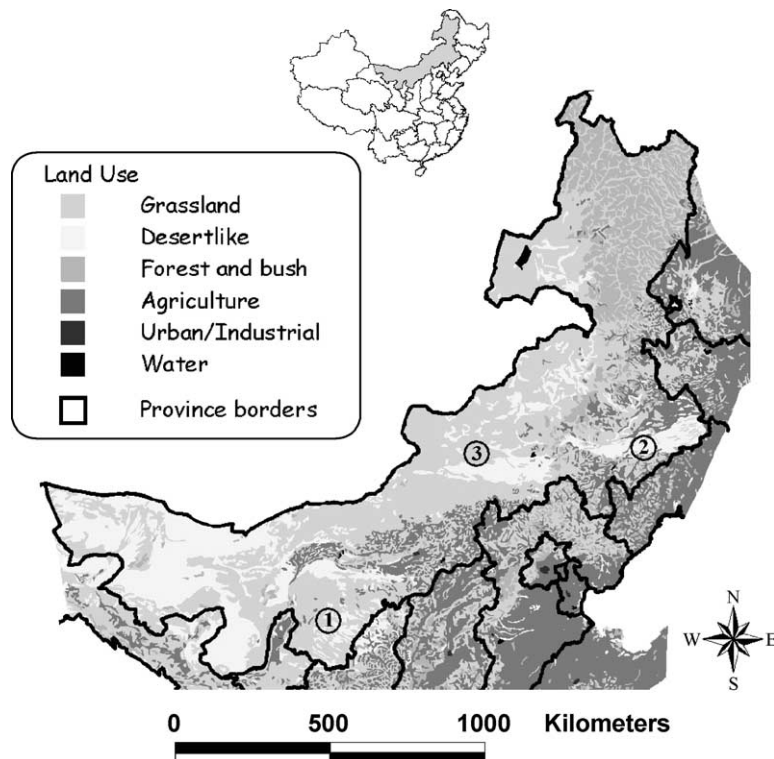


Fig. 1. Simplified land use of the Inner Mongolia Autonomous Region. The position of the two reference stations, Eutoke (1) and Naiman (2), and the evaluation site, Xilingol (3), are marked.

2.2. Data

The satellite data come from the Pathfinder Land (PAL) Data Set, a product derived from the NOAA AVHRR sensors (James and Kalluri, 1994). NDVI at monthly intervals and daily classifications of cloud cover from the CLOUDS AVHRR (CLAVR), at a spatial resolution of 8×8 km, have been used in this study. Data between 1982 and 1999 were used, except for a period from mid September through December in 1994 where no data were available. The PAL NDVI data set was found to be stable until the year 2000 when a rapid drop in NDVI is evident, possibly a result of a delayed overpass time for NOAA-14 (Eklundh and Olsson, 2003). The data set was also tested for north China dryland conditions by Runnström (2000) between 1982 and 1993, and was found reasonably stable.

Three tiles of PAL data, each containing 125×125 grid cells, covered the geographical extent of the IMAR. A digital elevation model (elev) was used, also available from the PAL data set having the same spatial resolution as NDVI and CLAVR. The NDVI data set was corrected for soil reflection by determining the NDVI for bare soil (NDVI=0.072). This soil reference value (SRV) was linearly scaled between bare soil grid cells and full vegetation grid cells, determined at NDVI=0.60. A 100% subtraction of SRV from NDVI was made for bare soil grid cells and a 0% subtraction of SRV for grid cells indicating total vegetation cover. This is a generalization and assumes that soils have the same reflection properties throughout the IMAR, which disregards variability in moisture, organic matter content, etc.

Climate data from 40 stations with monthly observations of precipitation and mean maximum and minimum temperatures were used to drive the hydrological component of the LUE model. Potential evaporation was available from two climate stations, Ganjig ($42^{\circ}56'N$, $122^{\circ}21'E$) and Wushen ($39^{\circ}06'N$, $109^{\circ}02'E$). Additionally, daily data from these two stations (e.g., solar radiation, sunshine hours and precipitation) were used for calibration purposes.

Maximum soil moisture storage (SM_{max} —computed from topsoil texture and soil depth) was taken from version 3.5 of the FAO (Food and Agriculture Organization) Digital Soil Map of the World (DSMW, version 3.5 1995). The map, which provides soil classification at 5-min latitude/longitude grid-cells, was re-coded to yield

estimates of soil moisture storage capacity to an impermeable layer, or to a depth of 100 cm.

2.3. Model overview and revision

The original model, developed for the African Sahel (Seaquist, 2001; Seaquist et al., 2004), has been partly improved and adjusted to fit the continental type of climate of the IMAR (grey boxes in Fig. 2). These include an improved method of estimating diffuse radiation for the PAR computation, an alternative formula for calculating potential evapotranspiration and a spatially more consistent procedure for the temporal downscaling of monthly precipitation. In addition, two temperature stress factors (ts_1 and ts_2) have been introduced as well as a temperature-based algorithm that estimates the proportions of C3/C4 in each grid cell, and C3 maximum photosynthetic efficiency (propC3) based on mean temperature. ws denotes the water stress factor and n the month of year. Eq. (1) is therefore expanded to Eq. (3):

$$\begin{aligned} GPP_{total} &= \sum_{i=1}^n [(propC3 \times epC3 \times ws \times ts_1 \times ts_2 \times APAR) \\ &+ (propC4 \times epC4 \times ws \times ts_1 \times ts_2 \times APAR)] \end{aligned} \quad (3)$$

Incident PAR is computed as a proportion of the potential global radiation (GR) that is adjusted according to daily cloud coverage classes from the NOAA PAL's CLAVR layer. Potential evaporation (PET) is partitioned into potential soil evaporation and potential transpiration through an estimation of vegetation fraction derived from NDVI. Evaporation from bare soil and potential transpiration are treated separately by a two-layer bucket model that gives an estimate of the impact of soil water stress on plant growth. The ratio between actual to potential transpiration yields the water stress term. In Eq. (3), APAR is multiplied by the water stress and temperature stress factors, and the computed proportions for the photosynthetic pathway and potential photosynthetic efficiency values. The GPP results are presented in $g\ m^{-2}$ of dry matter (DM) and represents both above and belowground production.

Both empirical and more mechanistic models of photosynthesis enable GPP to be predicted with some confidence, while the simulation of plant respiration has

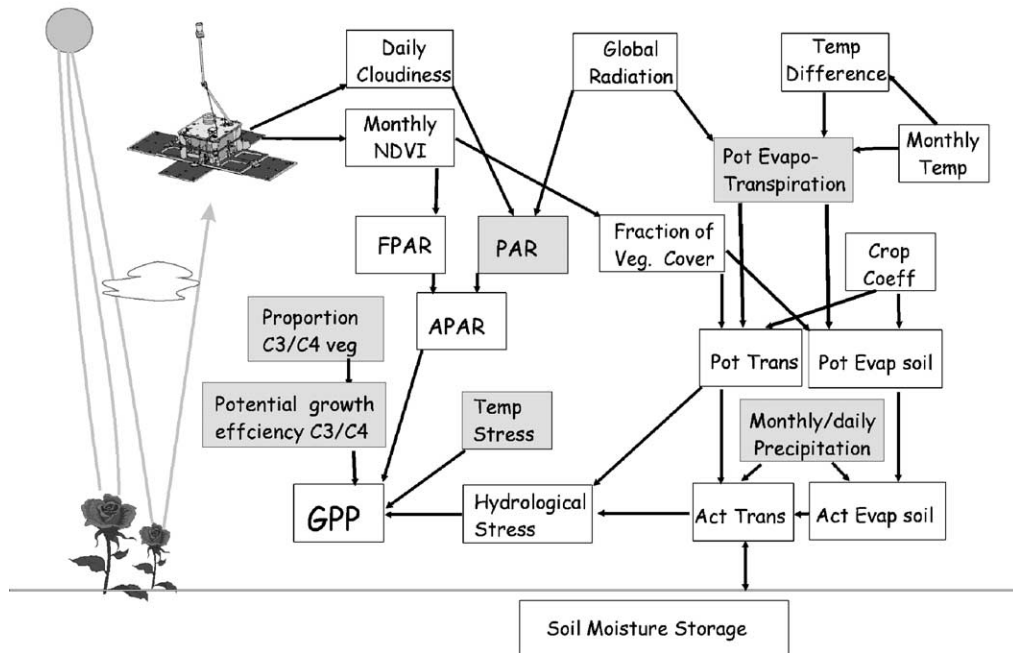


Fig. 2. Overview of the GPP model. Components that have been modified or added in the course of this work are highlighted in gray.

been less successful due to poorly understood processes though various approaches have been tested (Cannell and Thornley, 1999). Given that photosynthesis provides a basis for respiration, and there is a close coupling between the amount of carbon assimilated and that which is lost by respiration, the ratio of photosynthesis to respiration is fairly stable when averaged over weeks or longer. However, the ratio for a species may vary between different growing environments and the respiration fraction is likely to increase in plants that are water stressed leading to greater respiratory losses compared to the uptake of carbon. To allow for comparison with ground observations of net primary production at some sites, respiratory losses have been approximated as a fixed proportion of GPP at these sites.

2.4. PAR and APAR

Total incoming PAR was approximated being 48% of the short-wave flux (SW) (Frouin and Pinker, 1995), which was calculated with a model where daily estimates of GR at the top of the atmosphere were derived trigonometrically from grid cell-based latitude, solar declination, Sun–Earth distance, Julian day, day length and using a solar constant of 1372 W m^{-2}

(Monteith and Unsworth, 1990; Seaquist and Olsson, 1999). To estimate the amount of energy attenuated by the atmosphere, classifications of clear, cloudy or mixed conditions from the NOAA CLAVR data were analyzed at two reference stations. Compared to ground measurements of SW flux, the clear classification from CLAVR corresponded to an average of 61% penetration of radiation through the atmosphere, and mixed and cloudy grid cells to 47% and 40%, respectively (Runnström et al., 2004). The daily GR was reduced based on the grid cell-classification and the daily images were summed into monthly.

The fraction of PAR absorbed by the vegetation was estimated with the NDVI. Un-vegetated areas, such as sand (NDVI=0.00, after soil correction) were assumed to absorb no PAR, while maximum absorption (95%) was determined by the NDVI for irrigated areas (NDVI=0.60) representing full vegetation cover (Lind and Fensholt, 1999). Multiplying PAR and FPAR produced APAR.

2.5. The hydrological component

2.5.1. Precipitation and temperature

Monthly rainfall and monthly mean, mean maximum and mean minimum temperature records from 40

climate stations were interpolated spatially onto the same grid as the NOAA PAL data. Thirty-five stations are located within the inner Mongolian province border and five stations were included in surrounding provinces to minimize edge effects. A minimum curvature algorithm was used to interpolate both temperature and rainfall. The temperature data were recalculated to ‘at sea level’ by the dry adiabatic lapse rate ($0.6\text{ }^{\circ}\text{C}/100\text{ m}$) (Liljequist, 1970). After the interpolation, temperature surfaces were adjusted with the digital elevation model (elev).

2.5.2. Downscaling of precipitation

Interpolated rainfall series were temporally scaled down to simulate daily rainfall that is later needed for computing actual soil evaporation (see Section 2.5.4). Lacking daily data for all stations a downscaling algorithm was considered the best option to be able to fully apply the hydrological components of the LULUE model. Three magnitude categories of rainfall events were identified, small, medium and large based on altogether 15 years of daily data from Eutoke and Ganjig climate stations. The monthly frequency of these events for the rainy season was then determined. On average, 8 days of each month in the rainy season received rainfall of which four were small magnitude events, contributing 2% of the monthly rainfall, three were medium, each contributing 17% and one large event, the remaining 41%. The days that should receive rainfall were determined through a random-number generator grid cell by grid cell. The program

allowed several rainfall events to occur in the same grid cell in a month.

2.5.3. Potential evapotranspiration

PET was estimated with the Hargreaves method (Shuttleworth, 1993) (Eq. (A1)) and resulted in a good agreement (Fig. 3) with monthly data at the two control stations (Ganjig and Wushen). The improvement (compared to the Priestly and Taylor, 1972 method which was originally used in the Sahel model) is related to the inclusion of mean monthly maximum and minimum temperature differences in the Hargreaves algorithm, an important factor in a temperate climate. PET was partitioned into (1) potential transpiration and (2) potential soil evaporation by determining the fraction of vegetation in each grid cell through the NDVI (Eqs. (A2) and (A3)) (Carlson and Ripley, 1997; Choudhury and DiGirolamo, 1998).

2.5.4. Actual soil evaporation

The Ritchie (1972) model is used to compute actual evaporation from bare soil as a two-phase process. The actual evaporation is limited by energy (phase 1) and by soil hydraulic properties as a function of time (phase 2). The sum of phase 1 and phase 2 yields the actual evaporation from the soil (Eqs. (A4) and (A5)).

2.5.5. Actual transpiration and water stress

A bucket model (Eq. (A6)) computes daily cell-specific actual transpiration where the root zone is

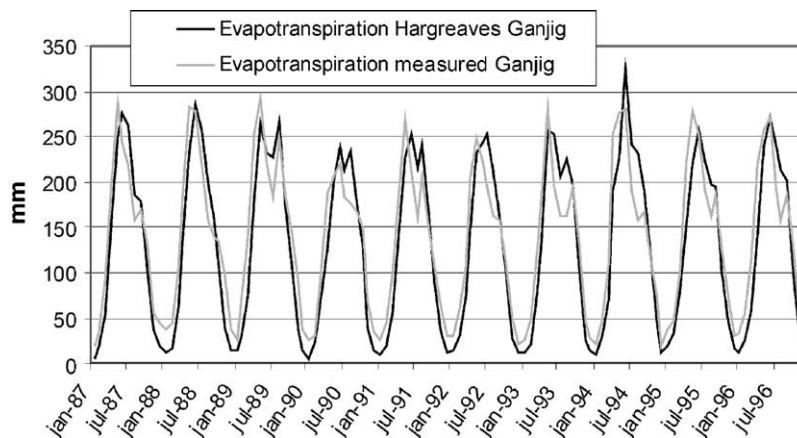


Fig. 3. Potential evapotranspiration, measured against modeled by Hargreaves method, at Ganjig ($42^{\circ}56'N$, $122^{\circ}21'E$) (Keerqinzuoyihou Banner National Economic Statistical Data, 1987–1997).

given in a single layer with maximum water holding capacity (SM_{max}). Summing daily actual transpiration into monthly values, the ratio between actual and potential transpiration constitutes the monthly water stress factor (Wight and Hanks, 1981; Srivastava et al., 1997). The ratio parameterizes the effect of low soil moisture on the stomatal conductance of vegetation, estimating the impact of water-stress affecting the vegetative fraction of the grid cell.

2.6. Temperature stress

To allow for the effects of temperature stress on C3 vegetation two temperature stress terms (Eqs. (A7) and (A8), respectively) suppressing ϵ (after Potter et al., 1993) have been applied. The first term (ts_1) serves to suppress ϵ at very high and at very low temperatures and the second term (ts_2) to suppress ϵ when the temperature is above or below the optimum temperature (t_{opt}). t_{opt} is defined as the mean monthly temperature when NDVI reaches its maximum. The ts_2 term reflects the concept that the light use efficiency should be suppressed when plants are growing at temperatures displaced from their optimum. The function is asymmetric bell-shaped and falls off more rapidly at high than at low temperatures.

2.7. Proportion of C3/C4 vegetation

Temperate grasslands can be partitioned according to their photosynthetic pathway, i.e., C3 or C4. Jiang et al. (1999a,b) investigated the photosynthetic response of different plant functional types to environmental changes along a northeast China transect where 48 out of 215 study species were C4 species. Lacking data for the IMAR, the observed relationship between the proportion of C4 grasses and temperature was used (Teeri and Stowe, 1976) (Eq. (A9)). In addition, a rainfall constraint on C4 vegetation was included (Berry, 1994) (see Appendix A).

2.8. Biological/photosynthetic efficiency values

For C4 vegetation, ϵ_p is not dependent on temperature and has a value of 6.1 g DM/MJ (equal to 2.76 g C/MJ if conversion factor for dry matter yield is assumed to be 0.45^{-1}). The gross ϵ for C3 plants is temperature-dependent and was calculated according

to Collatz et al. (1991), which is used by Prince and Goward (1995) and Goetz et al. (1999) (Eqs. (A10) (A11) (A12)).

3. Results and discussion

3.1. Annual mean, variability and trends of GPP

Modeled monthly GPP (above and below ground) were summed into annual values. These show a high degree of variability, temporally as well as spatially. From 1982 to 1999, mean annual GPP varies spatially from about 100 g/m² in desert regions in the west (e.g., Tenger and Ulan Buh) to about 4000 g/m² in the northeast of the IMAR, which are mostly forested (Fig. 4A). Although it is unclear how valid the LULUE model is for estimating biomass production in forested biomes with high leaf area index, estimates agree with plot-based measurements presented in Jiang et al. (1999a,b). Furthermore, the LULUE modeled GPP is only valid for natural rainfed vegetation. The spatial pattern of mean annual GPP in northern China is similar to the annual rainfall pattern, suggesting that seasonal rainfall amounts exert a dominant control on biological production in these environments, agreeing with conclusions drawn by Gao et al. (2001) and Cao et al. (2003). The inter-annual variability, the standard deviation for the 18 annual model observations divided by the mean and expressed as a percentage, was computed for each grid cell. Fig. 4B shows that the highest variability in annual GPP is found on the margins of the deserts in the west, where rainfall amounts are low and erratic. For these regions, years with higher rainfall results in a vegetation pulse in contrast to the dry years, which could explain the high variation. The linear slope of GPP was calculated in each grid cell to examine the spatial pattern of GPP trends, direction and magnitude, through the 18 years. The slopes vary considerably over the studied area and the standard deviation (σ) was 34 g/m² for the total study area covered (mean annual increase=+1.0 g/m² for number of pixels=46,875) for the total area and 33 g/m² for the IMAR region (mean annual increase=+3.3 g/m² for number of pixels=16,912) for the IMAR. Fig. 4C illustrates the spatial pattern of GPP trends, where grid cells were grouped by determining the departure of

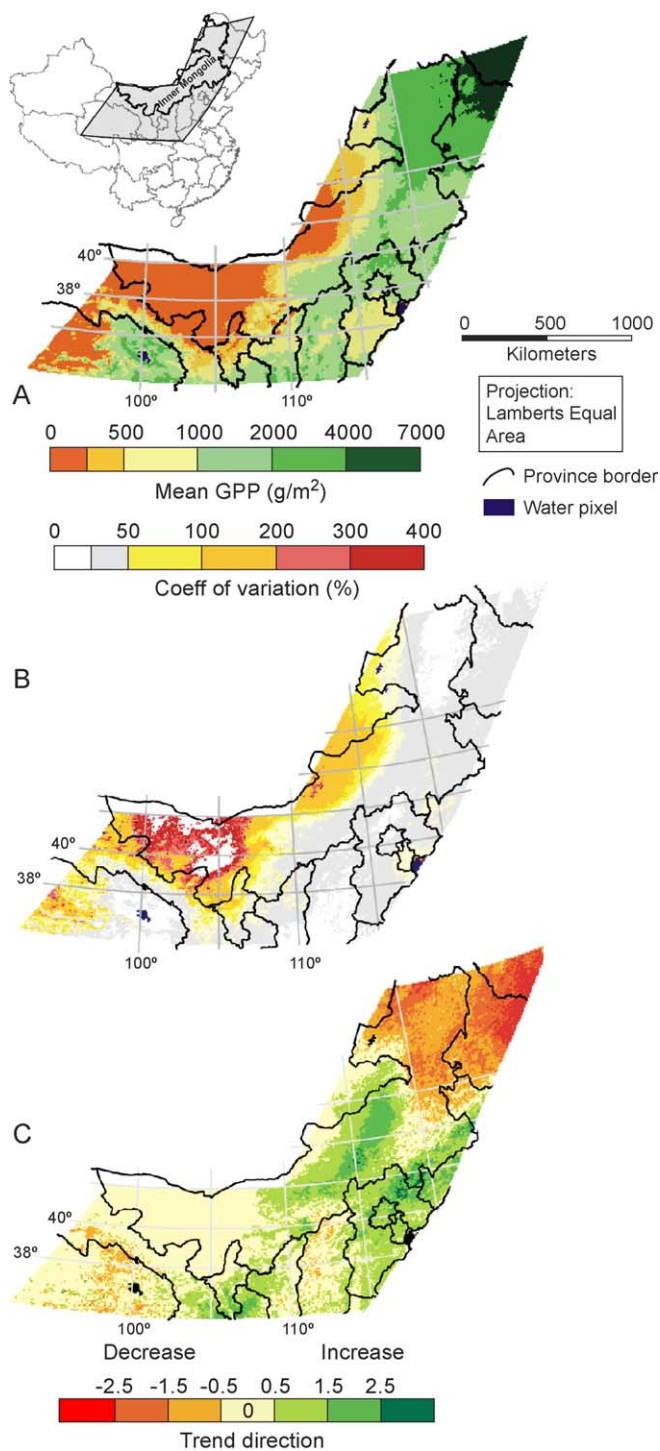


Fig. 4. Results from the model. (A) Mean GPP. (B) Coefficient of variation in GPP. (C) Trend of GPP between 1982 and 1999.

the slope from a zero trend, expressed in standard deviations ($\sigma=34$). The results are in line with Cao et al. (2003) who found a slight increase of primary production for the region in the period between 1981 and 1988. The significance of these trends were tested at the two reference stations (cf. Section 3.3), where trends were not significantly separated from zero. At the evaluation site, Xilingol, the trend was significantly positive. The greater magnitude of these slopes, the more likely the trends are statistically significant. The arid regions in the west have encountered low annual GPP and a no-change trend between 1982 and 1999. The northeastern regions show large negative trends that may indicate deforestation (e.g., Jiang et al., 1999a,b); however, the four climate stations available in this area all show declining precipitation through the time period. As the main goal has been to evaluate grassland production, the forested areas of the northeast will not be further discussed. A large area in the center, including the Xilingol site, has experienced high increase in primary production where correspondingly increasing trends of precipitation was registered by four climate stations. Of the 35 climate stations used in this study, 10 stations showed a 25% increase in mean seasonal rainfall (May–September), derived by fitting linear trends to these data, and two stations show a decrease of more than 25%. The mean summer temperature series (May–September) showed that for 23 stations, temperatures increased by more than 0.5 °C.

Despite a rapid increase in grazing animals on the steppes of the IMAR for the 1982–1999 period, our

model estimates do not indicate declining biological production. Although the cultivated land area constitutes only a small proportion of the total land area of the IMAR region, the findings of the primary productivity trends may be influenced by the increasing productivity of agricultural land. Other important factors contributing are the regional pattern of increasing precipitation over the 18-year period, as well as the *Green Wall* afforestation project and other vegetation cover improvement activities. The high inter-annual variability in primary production for this region makes it however difficult to identify long-term trends, despite the 18-year length of our record.

3.2. Evaluation

An evaluation of our results is difficult because of the lack of ground data representative of a 8-km resolution (Ustin et al., 1993). However, two methods were used to evaluate the accuracy and to compare the interannual variability of the model results. Measured grassland production between 1982 and 1989 on a 25-ha plot within the Xilingol biosphere reserve (43.72°N, 116.63°E) (USGS-NASA Distributed Active Archive Center, 2003a) was compared against our results for the corresponding grid cell (Fig 5). To make our modeled GPP comparable to the above-ground measured NPP for Xilingol, our GPP was multiplied by 0.75, the fraction of GPP remaining after growth respiration (Prince and Goward), and then by 0.64, the fraction of GPP remaining after maintenance respiration (Hunt, 1994). Finally, a ratio

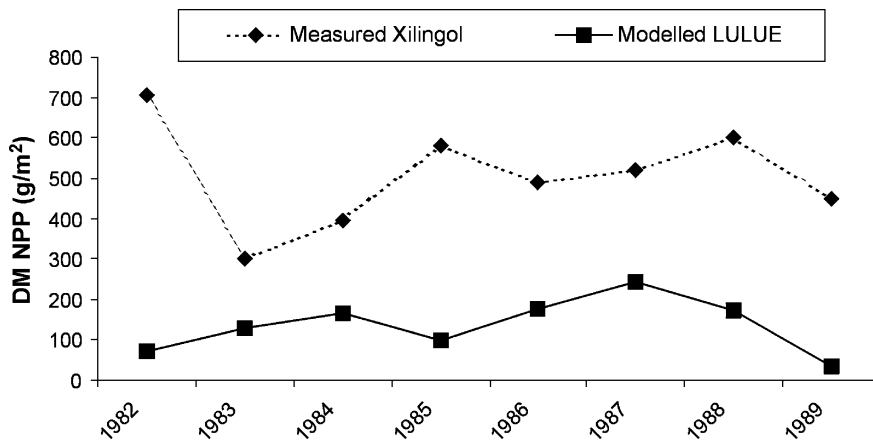


Fig. 5. Measured grassland production and model results for Xilingol (43.72°N, 116.63°E).

of 0.42 was used to isolate the aboveground NPP (AGNPP) (Gower et al., 1999). Measured amounts of NPP from Xilingol are higher than our results by a factor of about two and the correlation throughout the 9-year period is hardly significant. This seems logical as the Xilingol reserve represents only 0.4% of the grid cell size and has been excluded from any agricultural and grazing activities since 1980. Nevertheless, the range and variability in the model results lie within a similar magnitude.

In addition, a time-series of modeled production for one grid cell at the Eutoke site was evaluated against production estimates from the CENTURY model (Fig. 6). The CENTURY model is a general model of plant–soil nutrient cycling, which has been used to simulate carbon and nutrient dynamics for different types of ecosystems, e.g., grasslands (Parton et al., 1987; Metherell et al., 1993). The CENTURY model was driven with climate data from the Eutoke site, with medium grazing intensity, which is probable here, and was run for 2000 years prior to the 1982–1999 period to reach equilibrium for soil carbon. Our modeled NPP for the site was multiplied by 0.45 to convert to NPP Carbon. Regression between CENTURY and our model shows reasonable correlation for inter-annual variability ($r^2=0.32$, $n=18$), although they are about twice as high compared to CENTURY. NPP from the CENTURY model also have remarkably low inter-annual dynamic compared to our results and the measured Xilingol site. Both low variability and low actual NPP produced by CENTURY in drylands have also been identified by Seaquist (2001).

3.3. Analysis of controls on production

As the territory of Inner Mongolia is vast, the natural variability in environmental factors (as represented in the model) also vary. The obtained C3/C4 distribution, computed from Eq. (A9), reflects the climatic pattern of the study area. A higher proportion of the total photosynthetic gain by C4 plants is found in the southern parts of the area and at low elevations. In the dry, hot western part of IMAR, the C4 plant proportion reaches zero as water constraints sets in. This is in agreement with vegetation maps of this area (e.g., USGS-NASA Distributed Active Archive Center, 2003b), that classify the area as shrubs (C3 vegetation). Alternative algorithms, such as a purely temperature-based one used by Prince and Goward (1995), did not make this distinction and classified the same area as C4 vegetation.

Monthly values of the variables in Eq. (3) were extracted from the two reference grid cells for Naiman and Eutoke to identify dominant controls on primary production, and how they differ between two sites. Correlations between growing-season summed GPP and growing season summed values of these variables are presented in Table 1, together with mean values and coefficients of variability.

For Naiman, the variable giving the highest r^2 is by far the water-stress parameter, $r^2=0.84$, followed by the photosynthetic efficiency value of C3 vegetation with a $r^2=0.45$. The correlation with NDVI is 0.31, while the temperature stress (combined into one stress factor) and PAR correlations are not significant. In the dryer Eutoke, NDVI is the most positively correlated

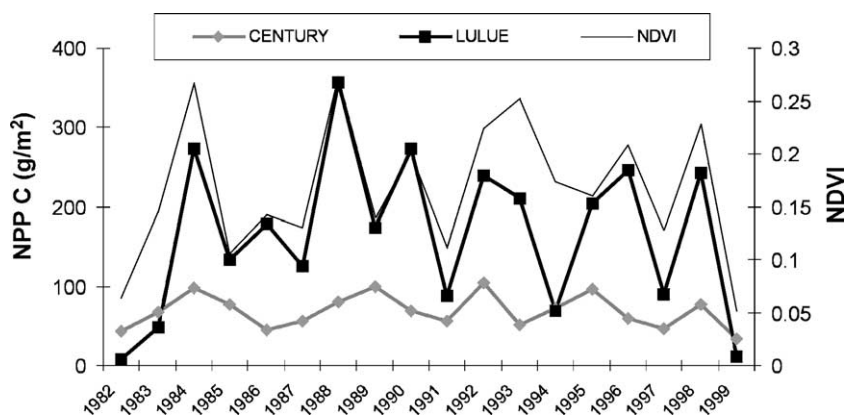


Fig. 6. Century, NDVI and model results for Eutoke reference site (39°05'N, 107°44'E).

Table 1

R^2 values resulting from correlations between estimated summed growing season GPP and growing season average values of different variables at the two reference sites

	Naiman			Eutoke		
	r^2 value between GPP and x	Mean value	Coefficient of variation (%)	r^2 value between GPP and x	Mean value	Coefficient of variation (%)
NDVI	0.31*	0.24	7.3	0.71***	0.11	33.3
PAR	-0.037	310	2	0.01	282	2.8
Water stress	0.84***	0.44	38.9	0.45**	0.52	41
Temperature stress	0.09	0.72	9	0.34*	0.8	4.3
ϵ potential C3 vegetation	0.45**	5.59	1.7	0.043	5.78	2.1

Asterisk indicates the significance of the correlations with a two-tailed test. Related data is the mean value for each variable and the coefficient of variability. Significance: *** $P < 0.001$, ** $P < 0.01$, * $P < 0.05$.

variable, $r^2=0.71$, followed by water stress with an $r^2=0.45$ and temperature stress correlation of 0.34. Neither C3 potential efficiency nor PAR correlations are significant at the Eutoke site. Seasonal summed NDVI has higher correlation with GPP in Eutoke compared to Naiman. This is partly due to the considerably higher coefficient of variation in NDVI for Eutoke, 33%, compared to Naiman, 7.3%, and because NDVI loses prediction capacity when $LAI > 3$. The higher correlations with water-stress in Naiman compared to Eutoke were unexpected as the rainfall in Naiman is higher, and the amount of water that can be stored in the soil according to SM_{max} also is higher (175 mm compared to 142 mm). However, the figures

should be regarded as relative in relation to other variables at one site, rather than to be used in comparisons between sites. That NDVI and the water stress variables resulted in high correlations in the dryland study area was expected, and is in line with previous studies on the importance of different drivers included in satellite driven primary production models (Potter et al., 1999.)

To further analyze the relation between NDVI and GPP for a broader precipitation and NDVI interval, two additional sites have been investigated (Fig. 7). At the Hailutu site ($41^{\circ}42'N$, $108^{\circ}31'E$), NDVI is low and annual average precipitation is only 165 mm, while in the Boketu area ($48^{\circ}46'N$, $121^{\circ}55'E$) NDVI

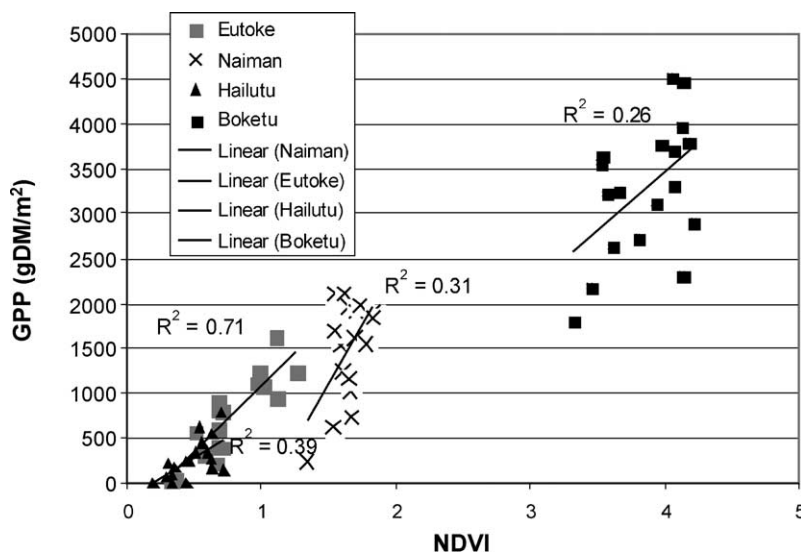


Fig. 7. The correlation between NDVI and LULUE modeled GPP at four sights in IMAR (annual average precipitation amounts in brackets): Eutoke (273 mm), Naiman (398 mm), Hailutu (165 mm) and Boketu (464 mm).

is high and the precipitation amounts to 460 mm. The highest correlation with between GPP and NDVI is found in Eutoke ($r^2=0.71$), while lower at the Naiman site ($r^2=0.31$), followed by Boketu ($r^2=0.26$). The Hailutu site in the dry northwest does not follow the pattern of increasing correlations with NDVI at drier sites. This can partly be explained by the low and erratic rainfall in the area resulting in a close to zero GPP computed by the model in some years. The difference in correlation between NDVI and primary production at the different sites points to the inappropriateness of using estimations of primary production based solely on NDVI over a large region.

To analyze the effects of the hydrological component of the model the inter correlation between rainfall and the water stress factor was tested, giving r^2 values of 0.25 and 0.064 for Naiman and Eutoke, respectively. The rather low values imply that the hydrological algorithms considerably change the temporal dynamics of soil moisture availability. One potential reason for the particularly low correlations at the Eutoke site is that the vegetation fraction is lower which makes the rainfall portion processed through the vegetative part of the hydrological model, and hence included in the water stress factor, considerably lower.

Apart from the hydrology component of the model, temperature drives both the temperature stress factor and the potential ϵ for C3. The average value and variability of monthly temperature stress is similar for the two sites, which is also the case for potential α for C3 vegetation. The two temperature-stress variables (ts_1 and ts_2) combined resulted in an average reduction from potential values over the growing season to 0.72 for Naiman and 0.80 for Eutoke with rather low variability between seasons of 9% and 4.3%, respectively. The temperature stress for the months of June, July and August were insignificant. In the early and late part of the growing season, temperature stress increases (due to cold) and GPP is reduced to about half of its amount. Finally, looking at the correlation between GPP and PAR, the r^2 values were low at both sites.

3.4. Time series of some variables

NDVI and water stress are the two most important driving variables when looking at both reference sites. Fig. 8 shows time series of NDVI and water stress in relation to modeled growing season GPP.

The closer relationship between accumulated GPP and NDVI in the Eutoke area (Fig. 8C) is striking, as is the closer relationship with water stress in the Naiman area (Fig. 8B). Mean seasonal GPP over the time period is 1500 g/m² in Naiman, compared to 750 g/m² for Eutoke, while the coefficient of variability is 37% and 60%, respectively. For Naiman, the linear trend through the modeled 18-year period shows an increase of nearly 30 g/m²/year, compared to less than 5 g/m² at Eutoke. Due to the large variability in seasonal GPP, the trend is not statistically significant for any of the sites. By comparison, the positive NDVI trend for Naiman, which has a much lower variability, is significant.

The findings for GPP for the two sites are presented in Table 2. Z-scores have been classified into five categories, where (++)/(--) denotes annual GPP above/below one standard deviations from mean and (+)/(-) denotes annual GPP above/below 0.5<1 standard deviations from mean. In Naiman, years with lower GPP are also characterized by high water stress (Fig. 5b). In the Eutoke area, the low GPP years have either high water stress or low NDVI values, or both, as these two are correlated with one another in a dryland area over longer periods. 1991 does not show particularly low NDVI values and only a moderate amount of water stress, but when examining the monthly data, rainfall is low throughout the growing season. In addition, the temperature constraint for this year is the highest for the 18-year period. Disaggregating seasonal precipitation and water stress into a monthly time step clearly reveals a time lag effect. High rainfall events carry over to the following month while prolonged drought aggravates the water availability situation in each successive month. The two sites show low growing season GPP in 1982 and 1983, with an improvement in 1984. At both sites, the combination of high water stress with low NDVI values and high temperature stress in 1982 results in low GPP estimates at the start of the time series. In the period 1985–1988, the two sites show different patterns in years of high and low rainfall. Years of higher productivity follow, with a decline in 1994. As NDVI is not available between August and December 1994, this period should be interpreted with caution. In 1997, both sites have low GPP, which improved in 1998, which was a year of extreme flooding in many regions of China, including the northeast. 1999 was

again a dry year, particularly in Eutoke where the biological production is low.

4. Summary and conclusions

Unlike other light use efficiency models that treat one grid cell uniformly independently of the vegetation cover, the LULUE model separately treats bare soil evaporation and actual transpiration, both at a quasi-daily time-step. We believe that this

refinement is more biophysically realistic and leads to enhanced precision in our water stress term, especially across vegetation gradients. The original model of primary production has been enhanced and adapted to the conditions of northern China changing the PAR computation as well as the temporal downscaling routine to produce quasi-daily rainfall estimates. In addition, two temperature stress factors have been introduced to complement the water stress factor, as well as algorithms to spatially compute C3/C4 photosynthetic pathway proportions

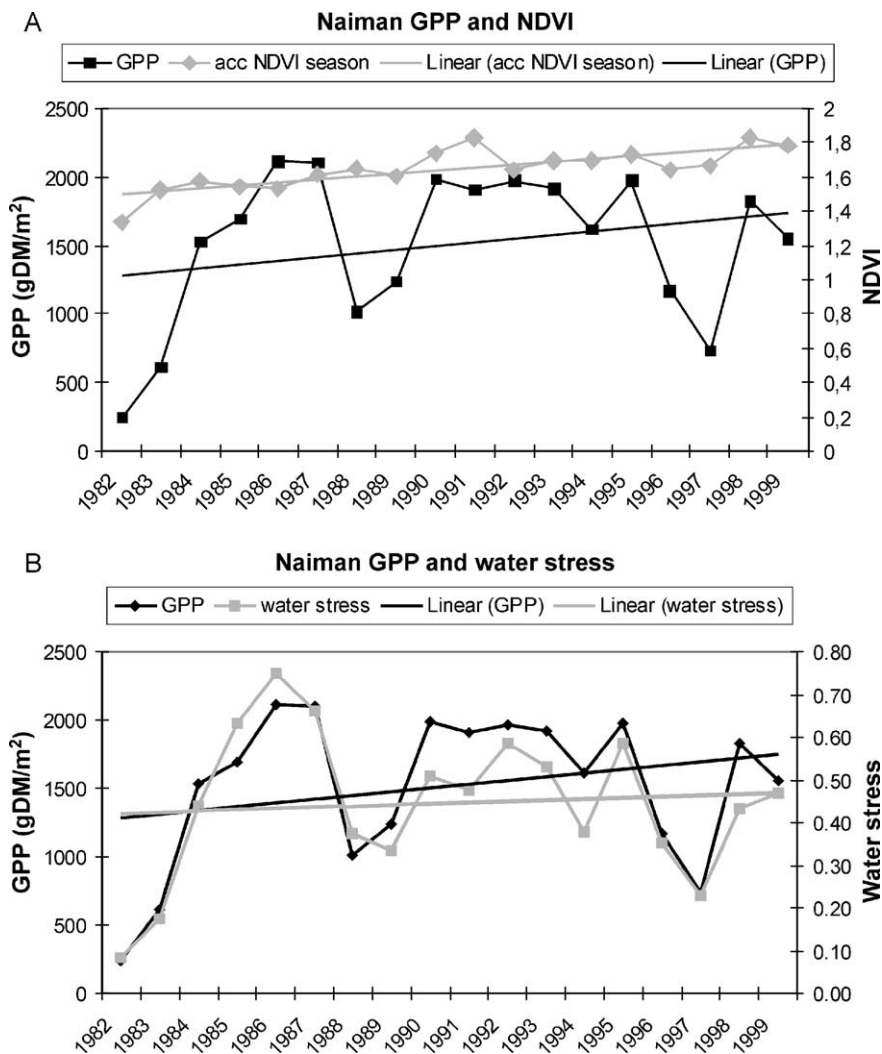


Fig. 8. (A–D) Time series of annual accumulated GPP in relation to accumulated NDVI and average water stress at the two reference sites Naiman and Eutoke. The water stress parameter is the fraction of actual transpiration to potential transpiration; hence, higher values denotes less stress.

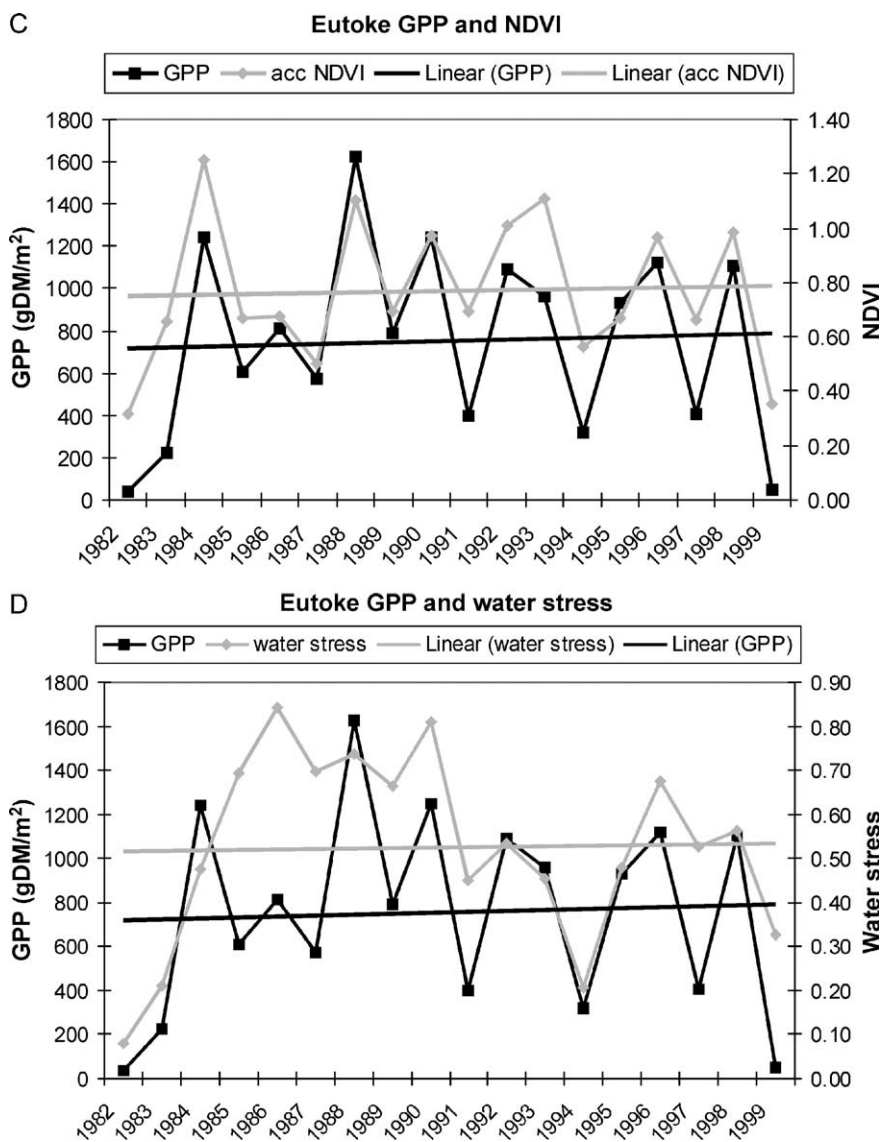


Fig. 8 (continued).

and temperature based C3 maximum efficiency values.

Mean annual modeled GPP ranges from about 100 g/m² in desert regions in the west (e.g., Tenger and Ulan Buh) to about 3400 g/m² in the northeast and the highest variability is found on the margins of the deserts in the west, where rainfall amounts are low and erratic. The fitting of linear trends

through the 18-year period reveal that the western regions show no change, while trends are negative for the northeastern part where rainfall has decreased. The central part of the IMAR shows a noticeable increase in GPP that coincides with increasing precipitation.

An evaluation of our results is difficult because the lack of corresponding ground-based data for

Table 2

Calculated Z-score values, i.e., the annual deviation from the mean divided by the standard deviation, for GPP from the two sites Naiman and Eutoke

	Naiman	Eutoke
1982	--	--
1983	--	--
1984		++
1985		-
1986	-	
1987	++	
1988	-	++
1989	-	
1990	+	++
1991	+	-
1992	+	+
1993	+	
1994		--
1995	+	
1996	-	+
1997	--	-
1998	+	+
1999		--

Vales have been classified where the annual GPP is more than one standard deviations from the 18-year mean (++ respective --), and between 0.5 and 1 standard deviations from mean (+ respective -).

grassland primary production representative for the 8-km pixel resolution. By comparing modeled results of annual primary production with above ground destructive measurements from the Xilingol biosphere reserve (0.4% of the pixel), and with CENTURY-modeled primary production at the Eutoke reference site, we conclude that our results are reasonable. They are lower than measured but higher than CENTURY. We also show that our model detects annual variability in the same range as the measured, as opposed to CENTURY, which produces very low variability. Furthermore, using NDVI alone as a relative indicator of production gave lower variability than our results as illustrated by the Naiman site where the coefficient of variation in GPP is 37%, NDVI 7.3% and water stress 39%. Corresponding figures for Eutoke are GPP 60%, NDVI 33% and water stress 41%.

For the two reference sites representing typical steppe vegetation of the Keerqin steppe (Naiman) and the Mu Us (Eutoke), the controls on production have been analysed. For both sites, the mean water stress and NDVI show statistically significant r^2 values against seasonally summed GPP, while potential ϵ for

C3 vegetation was statistically significant for the Naiman, and temperature stress for the Eutoke site, respectively. PAR was not significantly correlated with GPP at any of the sites.

Despite a rapid increase in grazing animals on the steppes of the IMAR for the 1982–1999 period, our model estimates do not indicate declining biological production. A combination of increasing crop yields, an increase in precipitation, as well as afforestation projects are likely factors explaining the pattern of regional increase in primary production.

Acknowledgment

Economic support for the study has been provided by the Swedish National Space Board, the Swedish Society for Anthropology and Geography, The Royal Swedish Academy of Sciences and Lund University Faculty of Sciences. The authors owe many thanks to Prof. Zhao Xueyong from the Cold and Arid Regions Environmental and Engineering Research Institute (CAS) for help during data collection and field visits, and to Liu Chunying for sharing climate data for Inner Mongolia. Thanks also to Drs. Lennart Olsson and Lars Eklundh for valuable comments on the manuscript. Data used by the authors in this study include data produced through funding from the Earth Observing System Pathfinder Program of NASA's Mission to Planet Earth in cooperation with the National Oceanic and Atmospheric Administration. The data were provided by the Earth Observing System Data and Information System (EOSDIS), Distributed Active Archive Center at Goddard Space Flight Center, which archives, manages and distributes this data set.

Appendix A

A.1. Potential evapotranspiration

$$\text{PET} = 0.0023 \times S_0 - \delta_T(T + 17.8) \quad (\text{A1})$$

PET (mm) is the potential evapotranspiration in mm/day, S_0 is the water equivalent of extraterrestrial radiation, T is the monthly mean temperature in

degrees Celsius and δ_T is the difference between mean monthly maximum and mean monthly minimum temperatures.

A.2. Partition of PET into bare soil and vegetation

$$PE = K_c * PET \left[1 - \left(\frac{NDVI - NDVI_0}{NDVI_s - NDVI_0} \right) \right] \quad (A2)$$

$$T_{pot} = K_c * PET \left(\frac{NDVI - NDVI_0}{NDVI_s - NDVI_0} \right) \quad (A3)$$

PE=potential evaporation from bare soil (mm), PET=potential evapotranspiration (mm), K_c =crop coefficient, T_{pot} =potential transpiration, NDVI=cell-specific NDVI, $NDVI_s$ =NDVI corresponding to full vegetation cover (0.6), $NDVI_0$ =bare soil NDVI (0.0).

The crop coefficient K_c was assigned a constant value of 0.85 in concordance with the typical mean growing season values for rangeland vegetation (Wight and Hanks, 1981; Seaquist, 2001).

A.3. Actual soil evaporation

$$\sum E_{s1} = \sum_{i=0}^{t1} PET_{s0} = U \quad t < t_1 \quad (A4)$$

$$\sum E_{s2} = k \times \sqrt{(t - t_1)} \quad t > t_1 \quad (A5)$$

where PET=potential evapotranspiration (mm), $\sum E_{s1}$ =stage 1 cumulative soil evaporation (mm), $\sum E_{s2}$ =stage 2 cumulative soil evaporation (mm), $\sum E_{s0}$ =potential evaporation for soil (mm), U =total amount of water evaporated setting the upper limit for phase 1 evaporation (mm), k =desorptivity (mm day⁻¹) (Ritchie, 1972; Wight and Hanks, 1981; Srivastava et al., 1997; Wallace and Holwill, 1997).

A.4. Bucket model for actual transpiration

$$T_{(t)} = SM_{(t-1)} + Rain_{(t)} - AE_{(t)} - SM_{(t)} - Runoff_{(t)} - Drainage_{(t)} \quad (A6)$$

where T =actual transpiration (mm), t =time step (day), SM=soil moisture (mm), Rain=rainfall (mm), AE=ac-

tual evaporation (mm) from the soil evaporation model, Runoff=water lost from the cell over the surface (mm), Drainage=water lost from the cell by drainage (mm).

Runoff and drainage are assumed relatively unimportant and are thus not treated (Wight and Hanks, 1981; Srivastava et al., 1997; Choudhury and DiGiralamo, 1998).

A.5. Temperature stress

$$ts_1 = 0.8 + 0.02t_{opt} - 0.005(t_{opt})^2 \quad (A7)$$

t_{opt} is defined as the mean temperature in the month of maximum NDVI. ts_1 ranges from 0.8 at 0 °C to 1.0 at 20 °C and to 0.8 at 40 °C.

$$ts_2 = 1.1814/1 + e^{[0.2(t_{opt}-10-T)]}/1 + e^{[0.3(-t_{opt}-10+T)]} \quad (A8)$$

ts_2 falls of to half of its value at t_{opt} at temperatures 10°C above or 13°C below T_{opt} .

A.6. Proportion of C4 vegetation

$$\begin{aligned} \text{PropC4} &= 0\% && \text{for } T < 5.94 \text{ }^\circ\text{C} \\ \text{PropC4} &= 0.0848T - 5.04 && \text{for } 5.94 \leq T \leq 17.80 \text{ }^\circ\text{C} \\ \text{PropC4} &= 100\% && \text{for } T > 17.8 \text{ }^\circ\text{C} \end{aligned} \quad (A9)$$

In addition to these limitations, a constrain on the distribution of C4 grasses was pointed out in Berry (1994) (in Lloyd and Farquhar, 1994), that the mean annual rainfall had to be at least 25 mm in a month of the year where the temperature was in excess of 22 °C was applied according to a modification of Lloyd and Farquhar (1994). According to them, this precipitation constrain was converted in proportion to the C4 proportion, i.e., for 50% of C4 grasses from Eq. (A9) the precipitation requirement was the occurrence of 12.5 in a month of the year where the mean monthly temperature was greater than 11 °C, with the other C4 proportions requiring a minimum precipitation depending on temperature accordingly.

A.7. Values of photosynthetic efficiency

$$\tau = 2600 * 0.57^{\left(\frac{T_a - 20}{10}\right)} \quad (\text{A10})$$

$$\Gamma^* = \frac{[\text{O}_2]}{2\tau} \text{ Pa} \quad ([\text{O}_2] = 20,900 \text{ Pa}) \quad (\text{A11})$$

$$\alpha = 0.08 \left(\frac{P_i - \Gamma^*}{P_i + 2\Gamma^*} \right) \text{ moles} * \text{mole}^{-1} \quad (P_i = 23.8 \text{ Pa}) \quad (\text{A12})$$

$$\varepsilon_{pC3} = 55.2 * \alpha * 0.45^{-1} \text{ g DM/MJ} \quad (\text{A13})$$

First the CO_2/O_2 specificity ratio (τ) is calculated (where T_a =mean temperature), followed by the CO_2 photocompensation point (Γ^*), then the quantum yield (α) and finally the potential efficiency values (ε_p) for C3 (Collatz et al., 1991).

References

- Berry, J.A., 1994. Global distribution of C4 plants. Carnegie Institute Washington Yearbook, 1992/93, pp. 60–64.
- Brogaard, S., Zhao, X., 2002. Rural reform and changes in land management and attitudes: a case study from Inner Mongolia, China. *Ambio* 31 (3), 219–225.
- Brown, L., 1995. Who Will Feed China? Wake-Up Call for A Small Planet. Earthscan, London, 159 pp.
- Cannell, J.H.M., Thornley, M.G.R., 1999. Modeling the components of plant respiration: representation and realism. *Annals of Botany* 85, 55–67.
- Cao, M., Prince, S.D., Li, K., Tao, B., Small, J., Shao, X., 2003. Response of terrestrial carbon uptake to interannual variability in China. *Global Change Biology* 9, 536–546.
- Carlson, T.N., Ripley, D.A., 1997. On the relation between NDVI, fractional vegetation cover, and leaf area index. *Remote Sensing of Environment* 62, 241–252.
- Choudhury, B.J., DiGirolamo, N.E., 1998. A biophysical process-based estimate of global land surface evaporation using satellite and ancillary data: I. Model description and comparison with observations. *Journal of Hydrology* 205, 164–185.
- Collatz, G.J., Ball, J.T., Griwet, C., Berry, J.A., 1991. Physiological and environmental regulation of stomatal conductance, photosynthesis and transpiration: a model that includes a laminar boundary layer. *Agriculture and Forest Meteorology* 54, 107–136.
- Cyranoski, D., 2003. China plans clean sweep on dust storm. *Nature* 421, 101.
- Eklundh, L., Olsson, L., 2003. Vegetation index trends for the African Sahel 1982–1999. *Geophysical Research Letters* 30 (8).
- FAO/UNESCO, 1995. Digital soil map of the world and derived properties. Version 3.5. Food and Agriculture Organization of the United Nations.
- Feng, Q., Endo, K.N., Cheng, G.D., 2001. Dust storms in China: a case study of dust storm variations and characteristics. *Bulletin of Engineering Geology and the Environment* 61, 253–261.
- Frouin, R., Pinker, R.T., 1995. Estimating photosynthetically active radiation (PAR) at the earth's surface from satellite observation. *Remote Sensing of Environment* 51, 98–107.
- Gao, Y., Fu, G., Yu, J., Yan, C., Niu, Z., Wang, C., 2001. Estimation of China net primary production by NOAA-AVHRR data. *IEEE* 0-7803-7/01, 1636–1638.
- Goetz, S.J., Prince, S.D., 1999. Modeling terrestrial carbon exchange and storage: evidence for and implications of functional convergence in light use efficiency. *Advances in Ecological Research* 28, 57–92.
- Goetz, S.J., Prince, S.D., Goward, S.N., Thawely, M.M., Small, J., 1999. Satellite remote sensing of primary production: an improved efficiency modeling approach. *Ecological Modeling* 122, 239–255.
- Goward, S.M., Hummerich, K.E., 1992. Vegetation canopy PAR absorptance and the normalized difference vegetation index: an assessment using the sail model. *Remote Sensing of Environment* 39, 29–51.
- Gower, S.T., Kusharik, C.J., Norman, J.M., 1999. Direct and indirect estimation of leaf area index, FPAR, and net primary production of terrestrial ecosystems. *Remote Sensing of Environment* 70, 119–140.
- Grassland and Grassland Sciences in Northern China, 1992. National Research Council U.S.A. National Academic Press, Washington.
- Ho, P.P.S., 2000. China rangelands under stress: a comparative study of pasture commons in the Ningxia Hui Autonomous Region. *Development and Change* 31, 385–412.
- Hunt, E.R., 1994. Relationship between woody biomass and PAR conversion efficiency for estimating net primary production from NDVI. *International Journal of Remote Sensing* 15, 1725–1730.
- James, M.E., Kalluri, S.N.V., 1994. The Pathfinder AVHRR land data set: an improved coarse resolution data set for terrestrial monitoring. *International Journal of Remote Sensing* 15, 3347–3363.
- Jiang, G., Tang, H., Yu, M., Dong, M., Zhang, X., 1999a. Responses of photosynthesis of different plant functional types to environmental changes along northeast China transect. *Trees* 14, 72–82.
- Jiang, H., Apps, M.J., Zhang, Y., Peng, C., Woodard, P., 1999b. Modeling the spatial pattern of net primary production in Chinese forests. *Ecological Modeling* 122, 275–288.
- Keerqinzuoyihou Banner National Economic Statistical Data, Yearbooks 1987–1997. Keerqinzuoyihou Banner Statistical Bureau, Ganjig. In Chinese.
- Law, B.E., Waring, R.H., 1994. Combining remote sensing and climatic data to estimate NPP across Oregon. *Ecological Applications* 4, 717–728.
- Liljequist, G.H., 1970. *Klimatologi*. Generalstabens Litografiska Anstalt, Stockholm (in Swedish).

- Lind, M., Fensholt, R., 1999. The spatio-temporal relationship between rainfall and vegetation development in Burkina Faso. *Danish Journal of Geography. Special issue 2*, 43–55.
- Lloyd, J., Farquhar, G.D., 1994. ^{13}C discrimination during CO_2 assimilation by the terrestrial biosphere. *Oecologia* 99, 201–215.
- Longworth, J.W., Williamson, G.J., 1993. China's Pastoral Region: Sheep and Wool, Minority Nationalities, Rangeland Degradation and Sustainable Development. CAB International, Wallingford, 352 pp.
- Metherell, A.K., Harding, L.A., Cole, C.V., Parton, W.J., 1993. CENTURY soil organic matter environment, Technical Documentation, Agroecosystem Version 4.0, US Department of Agriculture, Agricultural Research Service, Great Plains Research Unit. Technical Report #4.
- Monteith, J.L., 1972. Solar radiation and productivity in tropical ecosystems. *Journal of Applied Ecology* 9, 747–766.
- Monteith, J.L., 1977. Climate and the efficiency of crop production in Britain. *Philosophical Transactions of the Royal Society of London* 281, 277–294.
- Monteith, J.L., Unsworth, M., 1990. Principles of Environmental Physics, second edition. Edward Arnold, London, 291 pp.
- Myneni, R.B., Williams, D.L., 1994. On the relationship between FAPAR and NDVI. *Remote Sensing of Environment* 49, 200–211.
- Nemani, R.R., Keeling, C.D., Hashimoto, H., et al., 2003. Climate-driven increases in global terrestrial net primary production from 1982 to 1999. *Science* 300, 1560–1563.
- Ni, J., 2002. Carbon storage in grasslands in China. *Journal of Arid Environments* 50, 205–218.
- Nouvellon, Y., Seen, D.L., Rambal, S., Begue, A., Mora, M.S., Kerr, Y., Qi, J., 2000. Time course of radiation use efficiency in a shortgrass ecosystem: consequences for remotely sensed estimation of primary production. *Remote Sensing of Environment* 71, 43–55.
- Nyberg, A., Rozelle, S., 1999. Accelerating China's Rural Transformation. The World Bank, Washington D.C., 132 pp.
- Parton, W.J., Schimel, D.S., Cole, C.V., Ojima, D.S., 1987. Analysis of factors controlling soil organic matter levels in the Central Great Plains Grassland. *Soil Science Society of America Journal* 51, 1173–1179.
- Paruelo, J.M., Epstein, H.E., Lauenroth, W.K., Burke, I.C., 1997. ANPP estimates from NDVI for the Central Grassland Region of The United States. *Ecology* 78, 953–958.
- Potter, C.S., Randerson, J.T., Field, C.B., Matson, P.A., Vitousek, P.M., Mooney, H.A., Klooster, S.A., 1993. Terrestrial ecosystem production: a process model based on global satellite and surface data. *Global Biogeochemical Cycles* 7, 811–841.
- Potter, C.S., Klooster, S., Brooks, V., 1999. Interannual variability in terrestrial net primary production; exploration of trends and control on regional to global scale. *Ecosystems* 2, 36–48.
- Priestly, C.H.B., Taylor, R.J., 1972. On the assessment of surface heat flux and evaporation using large-scale parameters. *Monthly Weather Review* 100, 81–92.
- Prince, S.D., Goward, S.N., 1995. Global primary production: a remote sensing approach. *Journal of Biogeography* 22, 815–835.
- Rasmussen, M.S., 1998. Developing simple, operational, consistent NDVI-vegetation models by applying environmental and climatic information: Part I. Assessment of net primary production. *International Journal of Remote Sensing* 19, 97–117.
- Ritchie, J.T., 1972. Model for predicting evaporation from a row crop with incomplete cover. *Water Resources Research* 8, 1204–1213.
- Ruimy, A., Saugier, B., Dedieu, G., 1994. Methodology for the estimation of terrestrial NPP from remotely sensed data. *Journal of Geophysical Research* 99, 5263–5283.
- Running, S.W., Hunt Jr., E.R., 1993. Generalization of a forest ecosystem process model for other biomes, BIOME-BGC, and an application for global-scale models. In: Ehleringer, J.R., Field, C. (Eds.), *Scaling Processes Between Leaf and Landscape Levels*. Academic Press, pp. 141–158.
- Runnström, M., 2000. Is northern China winning the battle against desertification? *Ambio* 29, 468–476.
- Runnström, M., 2003. Rangeland development of the Mu Us Sandy Land in semiarid China: an analysis using Landsat and NOAA remote sensing data. *Land Degradation and Development* 14, 189–202.
- Runnström, M., Brogaard, S., Olsson, L., 2004. Estimation of PAR over Northern China in the context of NOAA AVHRR vegetation modeling. *Geocarto International* (in press).
- Seaquist, J., 2001. Mapping primary production for the West African Sahel with satellite data. *Meddelande från Lunds universitets geografiska institutioner, Avhandlingar* 140. PhD thesis, Department of Physical Geography, Lund University, Sweden.
- Seaquist, J.W., Olsson, L., 1999. Rapid estimation of photosynthetically active radiation over the West African Sahel using the pathfinder land data set. *International Journal of Earth Observation and Geoinformation* 1, 205–213.
- Seaquist, J.W., Olsson, L., Ardo, J., 2004. A remote sensing based primary production model for grassland biomes. *Ecological Modeling* 169, 131–155.
- Shuttleworth, W.J., 1993. Evaporation. In: Maidement, D.R. (Ed.), *Handbook of Hydrology*. McGraw-Hill, New York.
- Srivastava, S.K., Jayaraman, V., Nageswara Rao, P.P., Manikiam, B., Chandrasekhar, M.G., 1997. Interlinkages of NOAA/AVHRR derived integrated NDVI to seasonal precipitation and transpiration in dryland tropics. *International Journal of Remote Sensing* 18, 2931–2952.
- State Environmental Protection Administration, 2002. Report on the State of the Environment in China, Environmental Information Center, 2002.
- Statistical yearbook of Inner Mongolia, 1998. Chinas Statistical Publishing House. Beijing 1999.
- Teeri, J.A., Stowe, L.G., 1976. Climatic pattern and the distribution of C4 grasses in North America. *Oecologia* 23, 1–12.
- Thwaites, R., De Lacy, T., Hong, L.Y., Hua, L.X., 1998. Property rights, social change, and grassland degradation in Xilingol biosphere reserve, Inner Mongolia, China. *Society and Natural Resources* 11, 319–338.
- Tucker, C.J., Newcomb, W.W., Dregne, H.E., 1994. AVHRR data sets for determination of desert spatial extent. *International Journal of Remote Sensing* 15, 3547–3565.

- USGS-NASA Distributed Active Archive Center, 2003a. NPP Grassland: Xilingol, China, 1980–1989. http://www.daac.ornl.gov/NPP/site_des/xln_des.html, Access date 2003, May 2.
- USGS-NASA Distributed Active Archive Center, 2003b. The Euroasian land cover data base: Simple biosphere 2 Model Legend. http://edcdaac.usgs.gov/glcc/eadoc1_2.html#data, Access date 2003, May 2.
- Ustin, S.L., Smith, M.O., Adams, J.B., 1993. Remote sensing of ecological processes: a strategy for developing and testing ecological models using spectral mixture analysis. In: Ehleringer, J.R., Field, C.B. (Eds.), *Scaling Physiological Processes-Leaf to globe*. Academic Press, San Diego, 388 pp.
- Wallace, J.S., Holwill, C.J., 1997. Soil evaporation from tiger-bush in south-west Niger. *Journal of Hydrology* 188–189, 426–442.
- Wight, J.R., Hanks, R.J., 1981. A water-balance, climate model for range herbage production. *Journal of Range Management* 34, 307–311.
- Xiao, X., Wang, Y., Jiang, S., Ojima, D.S., Bonham, C.D., 1995. Interannual variation in the climate and above-ground biomass of *Leymus* Chinese steppe and *Stipa grandis* steppe in the Xilin river basin, Inner Mongolia, China. *Journal of Arid Environments* 35, 283–289.
- Yang, H., Li, X., 2000. Cultivated land and food supply in China. *Land Use Policy* 17, 73–88.
- Yusheng, W., Nishan, Z., Zhongru, X., 1991. The relationship between primary production and the major ecological factors and its predictions models in *Stipa baicalensis* steppe in northeast China. *Vegetatio* 96, 15–23.
- Zha, Y., Gao, J., 1997. Characteristics of desertification and its rehabilitation in China. *Journal of Arid Environments* 37, 419–432.
- Zhu, Z., Liu, S., Wu, Z., Di, X., 1986. *Deserts in China*. Institute of Desert Research. Academia Sinica Lanzhou, 132 pp.